



**HAL**  
open science

## Discrete-element simulations of comminution in rotating drums: Effects of grinding media

Luisa Fernanda Orozco, Duc-Hanh Nguyen, Jean-Yves Delenne, Philippe Sornay, Farhang Radjai

### ► To cite this version:

Luisa Fernanda Orozco, Duc-Hanh Nguyen, Jean-Yves Delenne, Philippe Sornay, Farhang Radjai. Discrete-element simulations of comminution in rotating drums: Effects of grinding media. Powder Technology, 2020, 362, pp.157-167. 10.1016/j.powtec.2019.12.014 . hal-02409236

**HAL Id: hal-02409236**

**<https://hal.science/hal-02409236>**

Submitted on 13 Dec 2019

**HAL** is a multi-disciplinary open access archive for the deposit and dissemination of scientific research documents, whether they are published or not. The documents may come from teaching and research institutions in France or abroad, or from public or private research centers.

L'archive ouverte pluridisciplinaire **HAL**, est destinée au dépôt et à la diffusion de documents scientifiques de niveau recherche, publiés ou non, émanant des établissements d'enseignement et de recherche français ou étrangers, des laboratoires publics ou privés.

# Discrete-element simulations of comminution in rotating drums: effects of grinding media

Luisa Fernanda Orozco<sup>a,b</sup>, Duc-Hanh Nguyen<sup>c</sup>, Jean-Yves Delenne<sup>d</sup>, Philippe Sornay<sup>a</sup>, Farhang Radjai<sup>b,\*</sup>

<sup>a</sup>CEA, DEN, DEC, SA3E, LCU, 13108 Saint Paul les Durance, France

<sup>b</sup>LMGC, CNRS, University of Montpellier, France

<sup>c</sup>Faculty of Hydraulic Engineering, National University of Civil Engineering, Hanoi, Vietnam

<sup>d</sup>IATE, INRA, CIRAD, Montpellier SupAgro, University of Montpellier, France

---

## Abstract

By means of Discrete-Element simulations with Bonded-Cell method for particle breakage, we investigate the evolution of crushable granular materials in a 2D rotating drum partially filled with heavy balls and powder grains. The grinding process with balls of different sizes or numbers is analyzed in terms of grain size and specific surface. The grinding rate is an increasing function of the number of balls, but, as a result of increasing energy dissipation by inelastic collisions between the balls, the process becomes energetically less efficient for larger number of balls. When the total volume of balls is kept constant, the ball size has generally little influence on particle breakage. We also introduce a model for the evolution of three size classes by accounting for the cushioning effect and transition rates between the classes. This model predicts an exponential decrease of the volume of large particles at the beginning of the process.

*Keywords:* Granular materials, Grinding, Ball mill, Discret-Element Method, Bonded-Cell method, Contact Dynamics Method

---

## 1. Introduction

Ball mills are widely used in agronomy, mining and pharmaceutical industries. The mixture of crushable particles with heavy balls introduced in a rotating hollow cylinder evolves by continuous size reduction as a result of the collisions of the balls (grinding media) with the particles (feed) [1, 2]. Several length scales are involved, ranging from ball-particle contacts to particle size, ball size, granular correlation lengths, and mill size. Hence, the amount of energy transmitted from the kinetic energy of the balls to the fracture of particles depends in a complex manner on the material and operational parameters of

---

\*Corresponding author

Email address: [franck.radjai@umontpellier.fr](mailto:franck.radjai@umontpellier.fr) (Farhang Radjai)

the process, which is notoriously inefficient [3, 4]. It has been estimated that in Australia, just in the mining sector, the grinding processes consume 36% of the total energy consumed by this sector, corresponding to 1.3% of Australia's energy consumption [5]. For this reason, understanding the behavior of granular materials in ball mills is crucial for the improvement of the operational conditions in view of the reduction of energy consumption.

Extensive studies have been reported on the performance of ball mills with respect to the choice of operational parameters, material properties, and milling conditions. Commonly, properties such as the particle size distribution, powder specific surface, powder density, breakage rate, collision energy and collision frequency are compared among different systems in order to evaluate the grinding energy efficiency and the particle size reduction properties [6, 7, 8, 9]. However, in many experimental studies of ball milling, the range of tested parameters is limited, and therefore inconclusive results are found. This gap may be filled by numerical simulations, which currently has its own challenge of reconciling numerical performance with the realism of the underlying physical model.

The population balance model (PBM) is a natural strategy that has been widely used for modeling the rate of change in the particle size distribution of materials subjected to comminution processes [3, 10, 11, 12, 13]. The particle breakage probability, a mass transfer function, and the breakage function or breakage rate are the three key components of this method. The breakage function is often determined by means of single particle breakage tests in which the load magnitude and the generated fragment size are linked [14, 15, 10]. The linear PBM considers a first-order or constant breakage rate during the process so that the breakage function depends only on the energy applied, particle size and some material properties [16]. Recent work on non-linear PBM intended to add a mechanistic effectiveness factor that takes into account the decrease of the breakage rate as the fines proportion increases [17]. Additionally, simulations of unbreakable spheres using the Discrete Element Method (DEM) have been performed in order to characterize the load transfer events that determine the breakage environments of the particles [18, 19, 20, 21]. Finally, the particle size distribution obtained using the PBM is often compared with experimental results in order to adjust the involved functions. However, these functions are material dependent and specific to a given set of operational conditions, requiring thus a calibration for every specific case [12].

For simulations based on the Discrete Element Method (DEM), several models of particle breakage have been developed and compared in [22]. Some use the Bonded Particle Method (BPM) in which the parent particle is composed of smaller spheres agglomerated [23]. Inside the drum, these agglomerates can break under load or due to collisions with unbreakable balls, walls, and other agglomerates. In a similar approach sometimes used, each particle is replaced by a collection of smaller spheres [24] or superquadrics [25] once a breakage criterion is achieved. Even though this process uses a progeny distribution model in which the particle volume is filled with smaller entities, a major drawback of such methods is that the particle volume is not conserved. As a matter of fact, the volume occupied by a dense agglomerate of mono-disperse spheres is

at least 40% larger than the sum of the volumes of its primary spheres [26].

The Bonded Cell Method (BCM) is an alternative approach in which the particles have a polygonal shape (or polyhedral in 3D) and they are tessellated into smaller polygonal cells [27, 28, 29]. Hence, there is no volume loss by body fragmentation of the particles. Moreover, as the cells touch along their sides (faces in 3D), the internal cohesion of the material can be accounted for in a more straightforward manner. In both BPM and BCM, the large number of fragments, treated within the DEM as regular particles, requires a compromise between the number of crushable particles and the number of primary particles or cells in each particle. But, as the internal stresses of the particles are correctly (up to discretization effect) calculated, they yield physically correct estimates of the evolution of size distributions if the debonding criterion is consistent with the classical framework of fracture mechanics, as discussed in [29]. For example, the effects of particle fracture on dilatancy and evolution of the distributions of particle sizes and shapes under shearing, the shattering effect, the slow reduction of the sizes of the largest particles as a result of cushioning effect (redistribution of stresses by smaller fragments) and the power-law distribution of intermediate fragments sizes are observed in the DEM-BCM simulations [30].

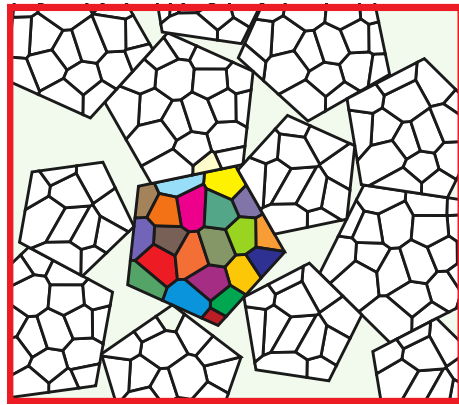
In this paper, we apply the BCM in 2D to investigate the ball milling process. The two-dimensional geometry of the system has the advantage of allowing us to work with a relatively large number of particles and cells for a meaningful statistics of fracture events and time evolution of the mixture in a rotating drum. The focus of this work is on the effects of the ball size and number on the fracture events in the granular material and the evolution of specific surface and particle size distribution. In contrast to most simulations previously reported on ball milling, we propose a systematic change of the parameters, allowing for a better understanding of the processes involved. We first introduce the BCM in the framework of the Contact Dynamics (CD) method. Then, we present the results of two groups of numerical simulations which are analyzed to evidence the effects of operational parameters on the evolution of particle size and specific surface as a function of the number of drum rotations. Finally, the tracking of particle breakage events and mass transfer between three size classes will be presented in order to get a more detailed understanding of the particle size reduction process. We conclude with salient results of this work and suggestions for further work.

## 2. Numerical method and procedures

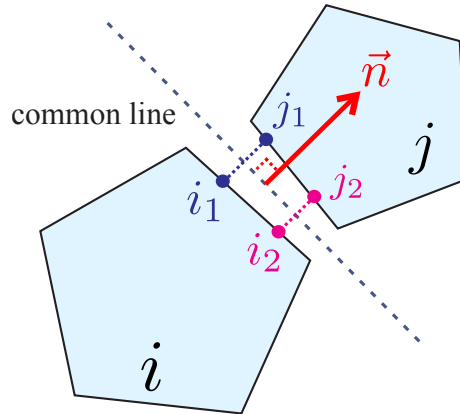
### 2.1. Bonded-Cell Method

In the BCM, each particle is modeled as an assembly of primary particles to which we will refer below as ‘cells’. Thus, when a particle breaks, the fragments generated are smaller particles each composed of cells. The smallest fragment is a single cell (representing the lower bound on fragment size). In order to define the cells configuration, a Voronoi tessellation is performed on each particle. The mean cell size  $d_{cell}$  is fixed so that a parent particle of surface  $s$  consists

of approximately  $s/d_{cell}^2$  cells. A parameter  $\kappa$  accounts for the cell shape heterogeneity, taking the value of 1 for very similar cell shapes, and 0 for very dissimilar cells. In previous work applying the BCM for particle breakage, it was found that setting  $\kappa$  close to 1 leads to nearly crystallized cell configurations with higher mechanical strength [28]. To avoid such effects, in this work  $\kappa$  is set to 0.5. The generated cells are convex polygons that are in side-side contact with their neighbors. Each parent particle is perfectly tessellated without defects or voids. Fig. 1(a) displays an example of a collection of pentagonal particles partitioned into irregular cells. For geometrical consistency, the crushable particles have a polygonal shape, too.



(a)



(b)

Figure 1: (a) Voronoi tessellation applied to polygonal particles. Each cell is presented in a different color; (b) Geometry of a side-side contact between two cells  $i$  and  $j$ . Two contact points (1 and 2) and their respective projections on the two cells, are defined for this type of contact.

Since the cells have polygonal shapes, various contact types can be expected: side-side, vertex-side, vertex-vertex. Initially, cohesive bonds are assigned to all side-side interfaces. Each side-side contact is represented by two distinct points belonging to their common contact line (point 1 and 2 with their respective projections on the body  $i$  ( $i_1, i_2$ ) and on the body  $j$  ( $j_1, j_2$ ), as shown in Fig. 1(b)). Initially, the common lines coincide with the common sides between cells as well as points 1 ( $i_1, j_1$ ) and 2 ( $i_2, j_2$ ). The common line also defines the contact normal  $\vec{n}$ .

Mechanically, an interface loses its cohesive status and becomes a fracture line if a local criterion is fulfilled. According to the classical fracture mechanics, this criterion should involve two ingredients: a stress threshold condition for crack initiation and an energetic propagation condition. We introduce three parameters: a normal stress threshold  $C_n$ , a tangential stress threshold  $C_t$  and an energy threshold  $\mathcal{W}$ . Since the cohesion acts at the side-side interfaces, the normal and tangential force thresholds for debonding are the products  $\ell C_n$  and  $\ell C_t$ , respectively, where  $\ell$  is the interface length. The critical energy for debonding can also be expressed in terms of a critical normal distance  $\Delta_n = \mathcal{W}/(\ell C_n)$  and a critical tangential distance  $\Delta_t = \mathcal{W}/(\ell C_t)$ . The two criteria along the normal and tangential directions to the interface are assumed to be independent. When a stress threshold is reached at a bond attributed to one of the two representative points of the interface, the interface remains cohesive but the two points are allowed to move during the next steps until the critical distance along the normal or tangential direction is reached. Then, the bond disappears irreversibly, corresponding to the propagation of a crack along the interface. When this occurs, the contact is treated as a non-cohesive frictional contact with friction coefficient  $\mu$ . The above debonding model can be described by the following inequalities:

$$\begin{cases} \varepsilon_n = 0 & \wedge & u_n = 0 & \Rightarrow & f_n \geq -C_n \ell \\ 0 < \varepsilon_n < \Delta_n & \wedge & u_n \geq 0 & \Rightarrow & f_n = -C_n \ell \\ \varepsilon_n > \Delta_n & & & \Rightarrow & f_n = 0 \end{cases} \quad (1)$$

$$\begin{cases} \varepsilon_t = 0 & \wedge & u_t = 0 & \Rightarrow & -C_t \ell \leq f_t \leq C_t \ell \\ 0 < \varepsilon_t < \Delta_t & \wedge & u_t \geq 0 & \Rightarrow & f_t = C_t \ell \\ -\Delta_t < \varepsilon_t < 0 & \wedge & u_t < 0 & \Rightarrow & f_t = -C_t \ell \\ |\varepsilon_t| > \Delta_t & & & \Rightarrow & \text{frictional contact} \end{cases} \quad (2)$$

where  $\varepsilon_n$  and  $\varepsilon_t$  are the normal and tangential distances between the representative points, and  $u_n$  and  $u_t$  denote the relative velocities in the normal and tangential directions, respectively.

Once a contact loses its cohesive state, the above cohesive behavior is replaced by a purely frictional behavior described by the following inequalities:

$$\begin{cases} u_n = 0 & \Rightarrow & f_n > 0 \\ u_n > 0 & \Rightarrow & f_n = 0 \end{cases} \quad (3)$$

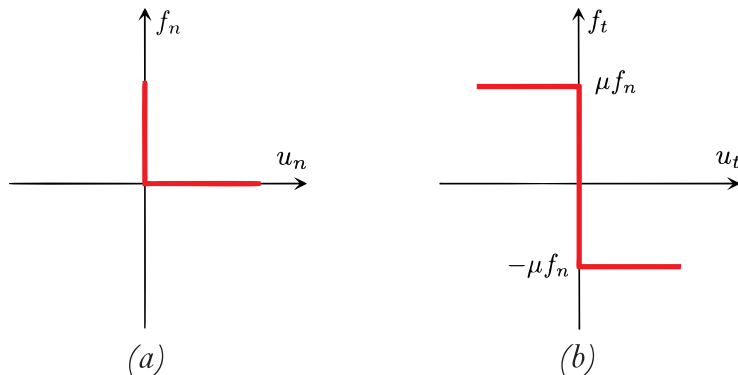


Figure 2: Purely frictional contact interactions: a) Relationship between normal force  $f_n$  and relative normal velocity  $u_n$  at a contact point; b) Coulomb friction law as a relationship between the friction force  $f_t$  and sliding velocity  $u_t$ .

$$\begin{cases} u_t = 0 & \Rightarrow & -\mu f_n \leq f_t \leq \mu f_n \\ u_t > 0 & \Rightarrow & f_t = \mu f_n \\ u_t < 0 & \Rightarrow & f_t = -\mu f_n \end{cases} \quad (4)$$

These inequalities are displayed as graphs in Fig. 2.

## 2.2. Contact Dynamics

The cohesive-frictional (eq. 1 and eq. 2) and purely frictional contact laws (eq. 3, eq. 4, and Fig. 2) are devoid of elastic strains. They describe a contact interaction independently of particle deformations. In this sense, they differ from the usual force laws used in DEM simulations where the contact strain is calculated from particle motions but is assumed to represent the elastic deflection at the contact point as in Hertzian contacts. The cohesive-frictional contact laws can be used with equations of motion in a time-stepping scheme, called Contact Dynamics Method (CDM), to determine the forces and velocities as in the more usual DEM [31, 32, 33]. The CDM belongs to the class of DEM models, but it implements the cohesive-frictional contact interactions without using elastic deflection at the contact points between particles. For this reason, it has been suggested that they should be discerned as *smooth DEM* for the usual DEM based on contact deflections, and *nonsmooth DEM* for CDM [34]. In contrast to smooth DEM, an implicit scheme based on an iterative Gauss-Seidel algorithm is used in CDM. This leads to unconditional stability of the time-stepping scheme, allowing therefore for larger time steps.

For the simulations we used a CDM-BCM algorithm implemented in the in-house GDM-tk software (see <https://www.cgp-gateway.org/Softwares/Gdm-tk/>). At each time step, the algorithm first performs a geometrical search for potential contacts. First, a rough selection of the neighbors is done for a search distance, followed by a narrower detection in which the positions of the geometrical features of the two candidates for contact are compared. Then, through an iterative process, the contact forces and particle velocities are simultaneously

Table 1: Parameters of the breakage model and material properties of powder particles and balls for all simulations

Variable	Value
$C_n$ (MPa)	1
$C_t$ (MPa)	0.4
$\mu$ (-)	0.4
$\Delta_n$ (m)	$5 \times 10^{-5}$
$\Delta_t$ (m)	$5 \times 10^{-5}$
$d_{cell}$ (m)	$5 \times 10^{-4}$
$\rho_p$ (kg/m <sup>3</sup> )	2000
$\rho_b$ (kg/m <sup>3</sup> )	11000

calculated for all the potential contacts. Finally, the positions are updated by using the calculated velocities. The initialization of the contact forces at the beginning of each time step with those found in the previous step reduces the degree of indeterminacy arising from the contact laws and the perfectly rigid nature of the particles, so that the variations between possible solutions are generally below the numerical precision [33].

### 2.3. Samples and setup

A hollow cylinder of an internal diameter equal to 15 cm is filled with powder (crushable particles) and balls. The ball density  $\rho_b$ , powder grains density  $\rho_p$  and mean voronoï cell size  $d_{cell}$  were fixed for all the tests. The density of the powder corresponds to that of uranium powder. The value of  $\rho_b$  typically used in the mining sector is  $\simeq 8000$  Kg/m<sup>3</sup> whereas for the manufacture of nuclear fuel powders the values are higher. Table 1 contains all parameter values including the breakage model parameters ( $C_n, C_t, \Delta_n, \Delta_t, \mu$ ). The values of  $C_n$  and  $\Delta_n$  were chosen such that the energy threshold  $\mathcal{W} = \ell C_n \Delta_n$  takes a value equal to 1 J/m<sup>2</sup>, often found for uranium dioxide [35, 36]. In all the simulations reported in this paper, we also take a smaller value of  $C_t$  ( $C_t/C_n = 0.4$ ), that favors fracture of particles in mode II.

An important characteristic of our model is that all the elements have polygonal shapes. The powder grains are pentagons while the balls are hexadecagons. The BCM together polygonal particle shapes allow us to choose arbitrary initial particle shapes [37]. However, the computational time for contact detection increases with the number of sides. For this reason, we used pentagonal shapes, which have a low number of sides and behave nearly like hexagonal particles. Lower number of sides (squares or triangles) are too specific and lead to pathological local structures [30]. The choice of pentagonal particle shapes is not a crucial parameter for milling since, as a result of particle breakage at the beginning of milling, a variety of different particle shapes are soon generated and therefore the evolution of grinding is mainly governed by a mixture of different particle shapes. The use of polydisperse pentagons prevents also from the creation of local crystallized structures often found in mono-disperse packings of hexagons and squares [37, 38, 39].

In general, the size of a polygonal particle is defined by the diameter of its circumscribed circle. The powder particles size are defined using a uniform particle volume fraction from  $d_{min} = 0.002$  m to  $d_{max} = 0.003$  m. Thus, given the cell size ( $d_{cell}$ ) adopted, the parent particles are composed of 16 to 36 cells. Finally, the simulation is run by applying a constant speed of 50 rpm to the cylinder for a total duration of 60 seconds. Fig. 3 shows several snapshots of a typical simulation.

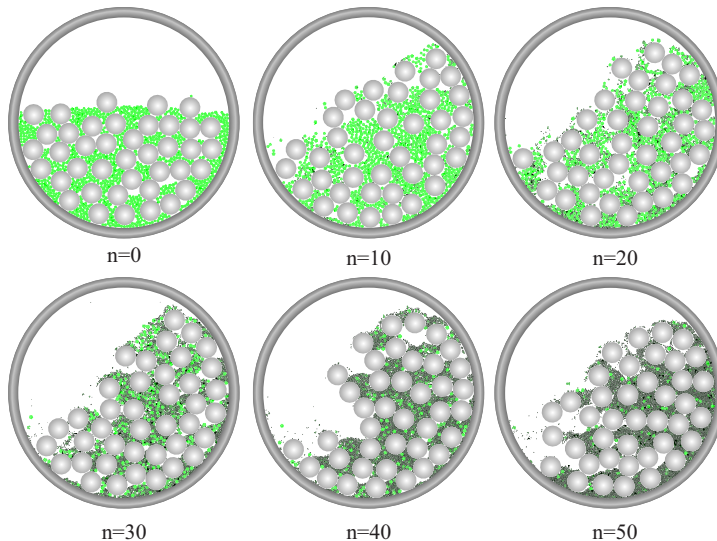


Figure 3: Snapshots of a ball mill system with ball size  $D_b = 15$  mm at different numbers  $n$  of drum rotations. The powder grain colors range from bright green (intact) to black (highly damaged).

The flow regime inside rotating drums is generally described in terms of the Froude number:

$$\text{Fr} = \frac{\omega^2 R}{g} \quad (5)$$

where  $\omega$  is rotation speed,  $R$  is drum's radius and  $g$  is the gravity [40]. For mixing applications, the rotating drums are operated under rolling or cascading regimes while for grinding applications the cataracting regime has been found more appropriate. In the cascading regime, the free surface of the flow exhibits a kidney S-shape while in the cataracting regime the particles flow along ballistic trajectories. In these two regimes, the flow is very rapid and the material behaves like a gas in which collisional particle interactions are highly present [41]. Because of the highly dynamic behavior, the transition between these two regimes is difficult to identify. In our simulations we set  $\text{Fr}=0.21$  for which the flow is in the cascading-ataracting regime.

Two case studies are considered in this work. In the first case, the effect of

Table 2: Geometrical characteristics of the two case studies

First case			Second case		
$D_b$ (mm)	$D_{drum}/D_b$ (-)	$D_b/\langle d_0 \rangle$ (-)	$N_b$ (-)	Filling degree (-)	$V_b/V_p$ (-)
5	30	2	10	21.43%	1.914
10	15	4	20	32.14%	2.829
15	10	6	25	39.29%	3.286
20	7.5	8	30	42.86%	3.743
25	6	10	50	67.86%	5.571

the ball diameter  $D_b$  is investigated whereas in the second case the number of balls  $N_b$  is varied. In the first case, five samples were built with a filling degree of 0.6, defined as the ratio of the apparent volume of the powder-balls mixture and drum's total volume. The diameter  $D_b$  is the same for all the balls in a given sample and it takes values of 5, 10, 15, 20 and 25 mm. The samples of this case are displayed in Fig. 2.3. Since the total volume  $V_b$  of the balls is constant, the number of balls decreases when the ball size is increased. Identical powder samples composed of 720 parent crushable particles are considered in all cases.

In the second case study, the ball size  $D_b$  was set to 15 mm for all simulations. As in the first case, the powder volume was kept constant and thus, the drums filled with different numbers  $N_b$  of balls have different filling degrees and values of the ratio  $V_b/V_p$ . In this case, the sample consists of 507 parent crushable particles. Snapshots of these samples are displayed in Fig. 2.3. Table 2 presents the geometrical properties of the two studied cases.

### 3. Effect of ball size

Figure 6(a) shows the mean powder grain size  $\langle d \rangle$  normalized by the initial mean size  $\langle d_0 \rangle$  as a function of the number  $n$  of drum rotations for different values of ball size  $D_b$ . The filling degree, total ball volume  $V_b$ , and total powder volume  $V_p$  keep the same values in all these simulations (see Fig. 2.3). Note that the particle diameter  $d$  of each fragment, which may have different shapes, is the *equivalent diameter*, i.e. the diameter of a disk having the same volume as the fragment. We observe slow size reduction during the first drum rotations. Then, the mean size  $\langle d \rangle$  declines almost exponentially down to a value close to cell size. The transient regime occurs more or less early depending on the ball size.

Figure 6(b) displays the evolution of the total specific surface  $S$  normalized by the initial specific surface  $S_0$  as a function of  $n$ . It increases nonlinearly with  $n$ , and, interestingly, apart from the two extreme values  $D_b = 5$  and  $D_b = 25$ , the plots coincide for all other values  $D_b$ . This behavior is consistent with the data points of Fig. 6(a) in which the evolution of  $\langle d \rangle$  for  $D_b = 5$  and  $D_b = 25$  is rather slow as compared to other diameters. We checked that the initial rise of specific surface in Fig. 6(b) (for the first drum rotations) is essentially due to damage caused by the creation of cracks inside the particles without causing

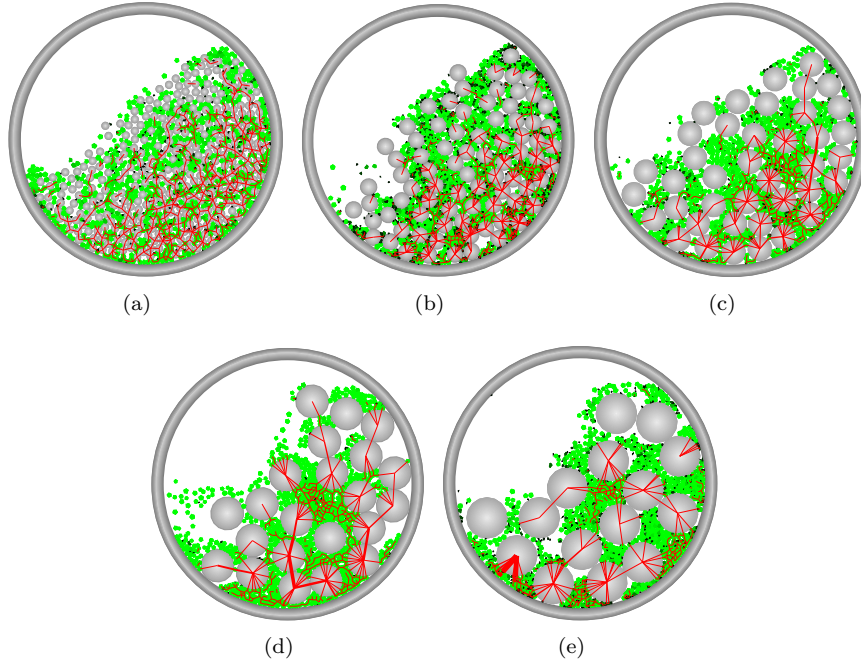


Figure 4: Snapshots of several simulations of systems with ball sizes  $D_b$  of a) 5 mm, b) 10 mm, c) 15 mm, d) 20 mm and e) 25 mm from left to right. The red line thickness is proportional to normal force.

grain rupture. For this reason, the specific surface grows initially at much higher rate than that of size reduction.

In the case of small ball size  $D_b$  ( $D_b/D_p = 2$ ), the milling process is similar to that of powder reduced by its own dynamics and without balls. Since the breakage events are concentrated at the downstream of the free surface, as observed in Fig. 7, the dominant breakage mechanism is the impact of particles (both powder particles and balls). Slow grinding occurs in this case due to the low inertia of the balls: smaller amounts of kinetic energy are carried by small balls in comparison to big balls, and therefore the impact energy is transmitted to the powder in small amounts. As noted by Erdem and Ergün [6], the small balls are suitable for reducing the small powder particles rather than the big ones, which are mainly broken by impacts of high collisional forces.

In contrast, with large ball size  $D_b$  ( $D_b/D_p = 10$ ), fewer impacts of higher magnitude occur [42]. As shown in Fig. 7, the high number of breakage events close to the drum wall is a consequence of the crushing of grains between the wall and a ball rolling down with a large amount of kinetic energy. This map shows also that many breakage events occur in the space between the balls with its signature as dense rings in the figure, which is a feature not observed for  $D_b = 5$  mm. However, the large ball size implies a large number of powder

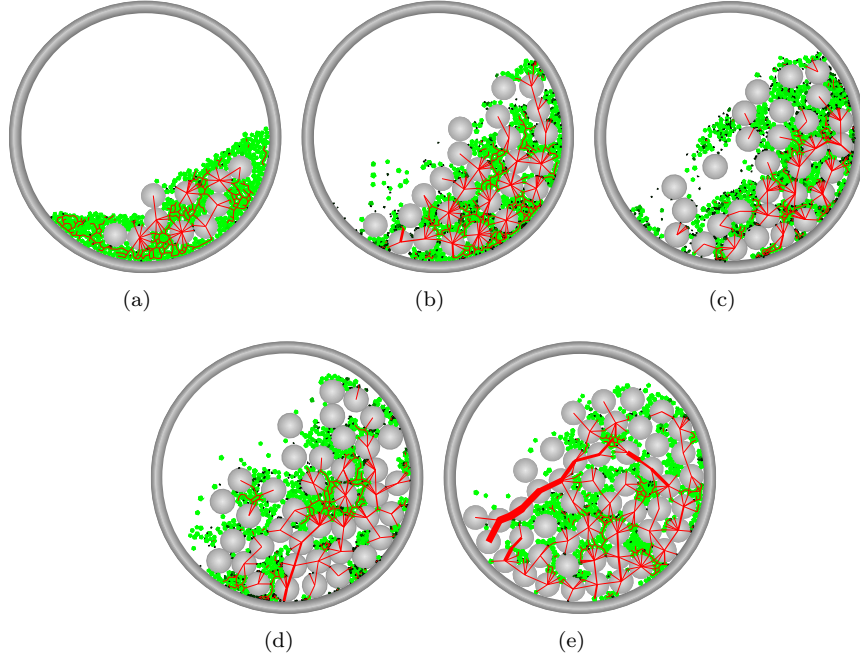
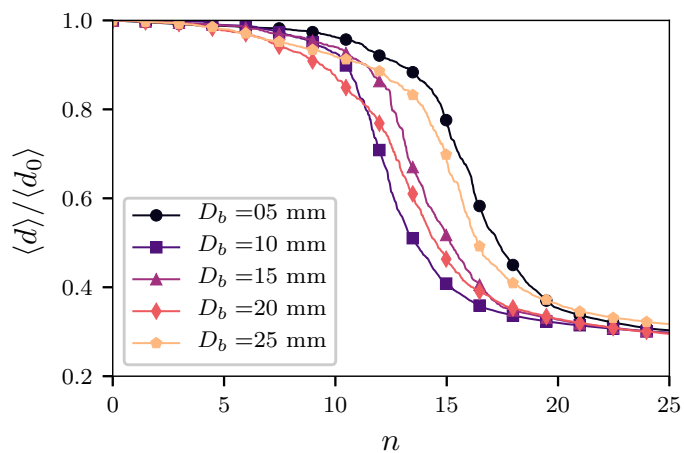


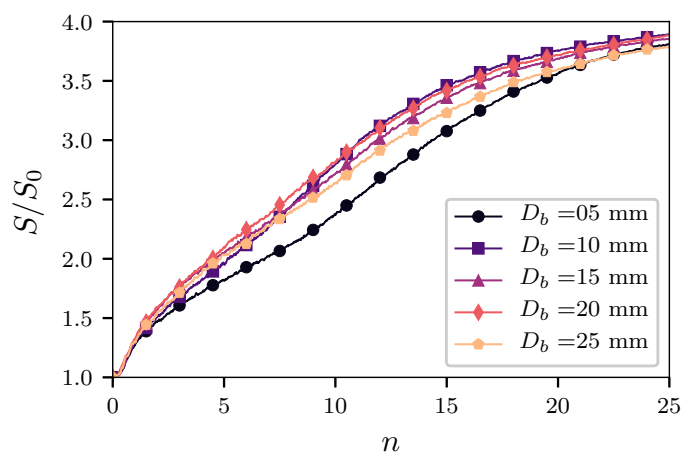
Figure 5: Snapshots of several simulations of systems with numbers of balls  $N_b =$  a) 10, b) 25, c) 30 d) 40 and e) 50, with  $D_b = 15\text{mm}$  constant. The red line thickness is proportional to normal force.

grains in the pore space between the balls. Many of these grains are floating and do not ‘feel’ large stress chains. A similar observation was made in [6].

To characterize in more detail these features, it is useful to consider the probability density function (pdf) of the interparticle forces. The pdf of forces between powder particles and balls is shown in Fig. 8(a) whereas Fig. 8(b) shows the pdf of the total force per ball at the beginning of grinding. The forces are normalized by the force threshold  $C_n\langle d \rangle$  for cell-cell debonding. The range of forces is quite broad, covering more than 10 decades. We observe two peaks, corresponding respectively to a very weak force value ( $f_n \simeq e^{-12}C_n\langle d \rangle$ ) and to a large force value ( $f_n \simeq e^{-12}C_n\langle d \rangle$ ). Only a few ‘critical’ forces are above  $C_n\langle d \rangle$  and can lead to particle fracture. The whole distribution will shift to larger forces if  $C_n$  is reduced. This will lead to the increase of the number of critical forces. The small force peak corresponds to the forces induced by grain weights whereas the large force peak reflects the dynamics of balls and ball-powder impacts, which is responsible for grinding. The amplitude of the large force peak decreases slightly as ball size increases as a result of the cushioning: the impulsive forces due to impacts are redistributed over a larger number of powder grains in contact with it. We see in Fig. 8(b) that the total normal force on the balls considerably increases due to this increasing number of ball-powder



(a)



(b)

Figure 6: Evolution with the number  $n$  of drum rotations of a) the mean particle size  $\langle d \rangle$  normalized by the initial mean diameter, and b) the specific surface  $S$  normalized by its initial value for different values of ball size  $D_b$ . The filling degree, total balls volume  $V_b$ , and powder volume  $V_p$  are constant. Each plot consists of 1000 data points.

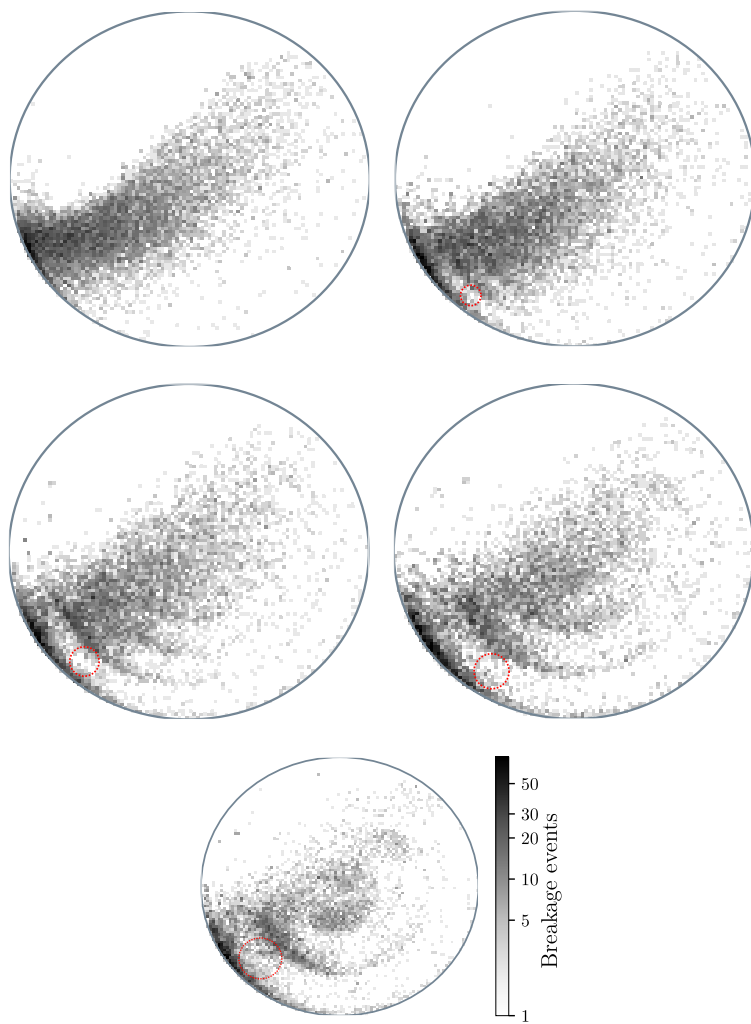


Figure 7: Spatial localization of breakage events in drums filled with balls of variable size  $D_b$ : 5, 10, 15, 20, 25 mm from left to right. The dashed red line represents the ball size of each case.

contacts.

Apart from the extreme ball diameters, the grinding evolution for all other ball diameters is nearly the same, with a slightly faster grinding for larger balls. This is a consequence of the fact that the total volume of balls is kept constant. As the kinetic energy is proportional to the volume, this almost independent behavior from ball diameter suggests that the surface created by milling is proportional to the kinetic energy. However, the breakage mechanisms that take place inside the drum change gradually with ball size. As mentioned previously and clearly observed in Fig. 7, the attrition of powder grains between grinding balls becomes increasingly more important as compared to impacts at the free surface when ball size increases.

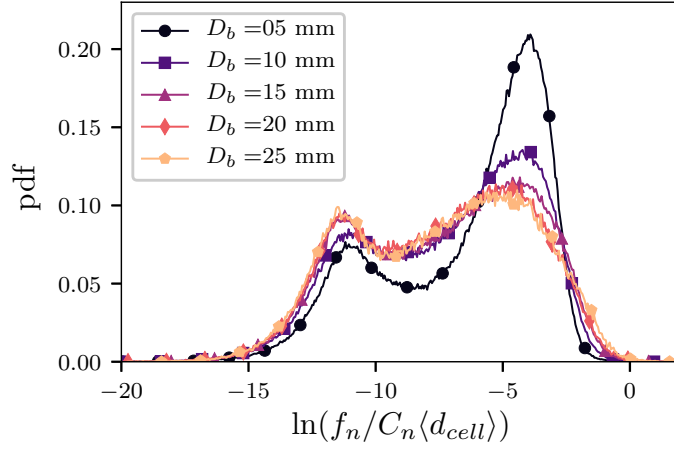
#### 4. Effect of the number of balls

Figures 9 and 10(a)(a) show the evolution of the mean powder particle size and specific surface, respectively, with the number of revolutions  $n$  for different values of the number of balls  $N_b$ , but at constant ball size  $D_b = 15$  mm and total powder volume  $V_p$ . The grinding curves change in an unmonotonic manner: it is increasingly faster as the number of balls increases from 10 to 30, but for larger numbers of balls the grinding becomes slower. The grinding rate  $\dot{S}$  is shown during the first 20 drum rotations is shown in Fig. 10(b), where we see the unmonotonic dependence of  $\dot{S}$  as a function of  $N_b$ . The largest rate occurs for  $N_b = 30$ .

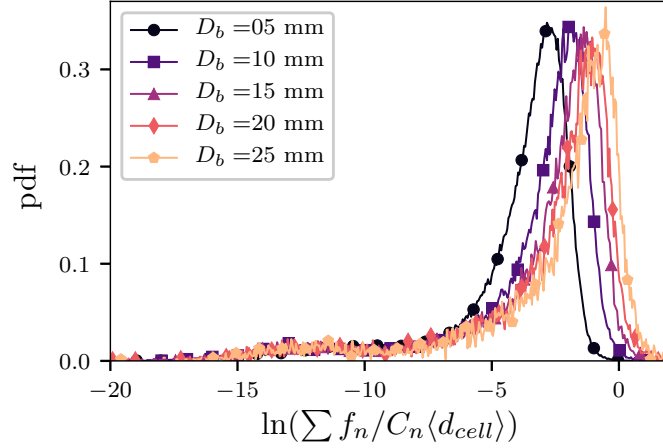
The nearly linear increase of the grinding rate with the number of balls during the first drum rotations naturally reflects the linear increase of the total volume of the grinding balls and thus their kinetic energy. However, as the total number of balls increases, the frequency of their mutual collisions increases, and thus an increasing amount of energy is dissipated by such inelastic collisions. For large number of balls, they may even undergo multiple collisions, in which case the stresses can be directly transmitted to the drum wall. An example is shown in Fig. 11 for  $N_b = 50$ , where we observe such chains of impulsive forces. Note also that in the other extreme case of  $N_b = 10$ , the kinetic energy is not sufficient to reach the lowest fragment size as those obtained with larger numbers of balls.

#### 5. A ternary population balance model

A full description of the grinding process in a ball mill requires the rates of volume transfer from each particle size class or population to all the classes of smaller size. This rate matrix is, however, statistically too rich to be determined from simulations with only a few thousand particles. For this reason, we consider three size classes between the initially largest particle diameter  $d_0^{max}$  and the smallest cell diameter  $d_{cell}^{min}$ . We divide this interval into three equal subintervals to which we refer below as “big”, “medium”, and “small” particles or size classes. These subintervals will be denoted by  $b$ ,  $m$ , and  $s$ , respectively. We are interested



(a)



(b)

Figure 8: Probability density function of normal forces  $f_n$  between the balls and powder grains (a), and the sum of the forces per ball (b), for different value of ball diameter  $D_b$  and normalized by the cohesion force  $C_N d_{cell}$ .

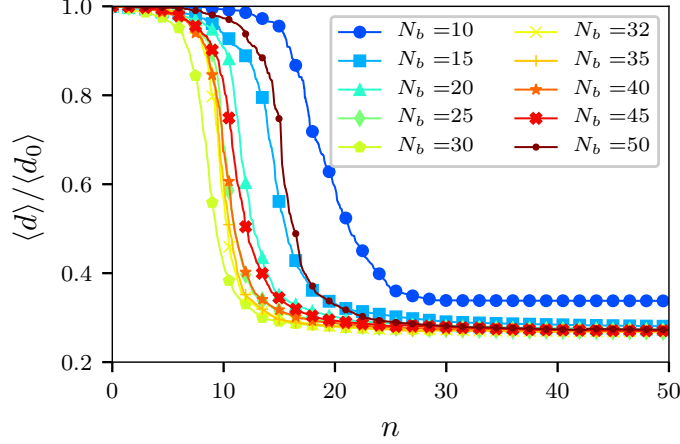


Figure 9: Evolution of the normalized mean particle size with the number of drum rotations for different numbers of balls  $N_b$ . The ball size  $D_b$  and powder volume  $V_p$  are constant. Each plot consists of 1000 data points.

in the evolution of the volumes  $V_b$ ,  $V_m$ , and  $V_s$  of these classes. The total volume of the particles

$$V = V_b + V_m + V_s \quad (6)$$

is conserved but the volume of each class evolves as a result of particle breakage. Since the breakage is irreversible, the transfer of volume can only occur from each size to smaller sizes:  $b \rightarrow m$ ,  $b \rightarrow s$  and  $m \rightarrow s$ . Figs. 12(a) and 12(b) show the time evolution of  $V_b$ ,  $V_m$  and  $V_s$  for two different numbers of balls together with fitting forms obtained from a simple model proposed below. At each time step of the simulation, we calculated the volume transferred between classes:  $\tau_b^m$  for volume transfer  $b \rightarrow m$ ,  $\tau_b^s$  for volume transfer  $b \rightarrow s$  and  $\tau_m^s$  for volume transfer  $m \rightarrow s$ . The cumulative values of volume transfer are plotted in Figs. 13(a) and 13(b).

At the beginning, nearly all particles belong to the class  $b$ . But in the course of grinding  $V_b$  declines monotonously whereas  $V_s$  increases. The volume  $V_m$  of the medium class has a nonmonotonic evolution. It begins to increase due to the breakage of big particles into medium ones ( $\tau_b^m$ ). In parallel, Fig. 13(b) shows that both  $\tau_b^m$  and  $\tau_m^s$  start increasing at a similar rate with a lag between them, that is small for  $D_b = 15$  but slightly larger for  $N_b = 32$ . This implies that the two volume transfers occur simultaneously and therefore  $V_m$  gradually tends to its maximum value  $\simeq 0.2V$  before decreasing. Also at this point  $V_b \simeq V_s = 0.4V$ . Another event occurs when  $\tau_b^m$  and  $\tau_m^s$  curves cross each other and  $V_b \simeq 0.2V$ . From this point on,  $\tau_b^m$  levels off due to a lack of big particles. The breakage rate  $\dot{\tau}_m^s$  of medium particles also decreases, but as  $\dot{\tau}_b^m < \dot{\tau}_m^s$ ,  $V_m$  starts to decrease. In Figs. 13(a) and 13(b) it is also remarkable

that the generation of small particles directly from big ones, by shattering or erosion, is less frequent than the two other volume transfers. When the mill starts rotating, some breakage events take place at the core section in which particles are mostly sheared. Once the granular flow is stabilized, the particles tumble and their ballistic trajectories lead to high-energy impacts with the walls and with other particles. Under such conditions the particles undergo mainly body fragmentation by generating either small particles from medium ones or medium particles from big ones.

The evolution of the three populations of big, medium and small particles can be described by means of detailed balance equations. Hence, we introduce the following rates: rate of change per unit volume  $\lambda_b^m$  from  $b$  to  $m$ , rate of change per unit volume  $\lambda_b^s$  from  $b$  to  $s$ , and rate of change per unit volume  $\lambda_m$  from  $m$  to  $s$ . We also set  $\lambda_b = \lambda_b^m + \lambda_b^s$ , the total rate of change per unit volume of big particles. We have

$$\begin{cases} \lambda_b^s = \frac{\tau_b^s}{\Delta t V_b} \\ \lambda_b^m = \frac{\tau_b^m}{\Delta t V_b} \\ \lambda_m = \frac{\tau_m^s}{\Delta t V_m} \end{cases} \quad (7)$$

The rate of change  $dV_b/dt$  of the volume of big particles at time  $t$  is proportional to their volume  $V_b(t)$ . If we assume that  $\lambda_b$  is constant, we have  $dV_b/dt = -\lambda_b V_b$ , which leads to an exponential decay of  $V_b$ . This trend is very close to what we observe in Figs. 12(a) and 12(b) except for the beginning of the curve. But even by ignoring the beginning of the curve, where the drum flow is not yet fully stabilized, the evolution is not exactly exponential. Hence, the rate is not constant and evolves during milling. Physically, we expect a gradual decrease in the fragmentation rate of big particles as a result of the generation of finer particles that tend to redistribute and hence reduce the forces acting on the big particles. This phenomenon is known as the *cushioning effect* [43, 16, 44, 17] or *hydrostatic effect* [45]. To account for this effect, we assume that the rate declines as an exponential function  $e^{\alpha_1(1-V_b/V)}$  of the volume of finer particles  $V - V_b$ . As  $V_b$  increases, this cushioning factor decreases. We apply the same effect to the medium particles whose volume  $V_m$  changes by a gain of volume as a result of the fragmentation of big particles and loss of volume by their own fragmentation. Hence, the system of partial differential equations for the three populations takes the following form:

$$\begin{cases} \frac{dV_b}{dt} = -\lambda_b V_b e^{\alpha_1(1-V_b/V)} \\ \frac{dV_m}{dt} = \lambda_b^m V_b e^{-\alpha_2(1-V_b/V)} - \lambda_m V_m e^{-\alpha_3 V_s/V} \\ V_s = V - V_b - V_m \end{cases} \quad (8)$$

where  $\alpha_1$ ,  $\alpha_2$  and  $\alpha_3$  are model parameters.

These equations provide an excellent fit of the three curves in Figs. 12(a) and 12(b) when their initial parts are excluded. The coefficients  $\lambda_b^m$ ,  $\lambda_b^s$ , and  $\lambda_m$  were obtained from the measurements of the volume transfers between populations and equation 7. The values of the model parameters found for the two cases are given in Table 3. Note that the low value of  $\alpha_1$  indicates that the decay of  $V_b$

Table 3: Values of the model (eq. 8) parameters found for the two studied cases in this section.

	$D_b = 15$	$N_b = 32$
$\lambda_b^m$	0.095	0.133
$\lambda_b^s$	0.018	0.025
$\lambda_b = \lambda_b^m + \lambda_b^s$	0.113	0.158
$\lambda_m$	0.150	0.187
$\alpha_1$	0.038	0.038
$\alpha_2$	1.2	1.47
$\alpha_3$	1.2	0.87

is actually very close to a purely exponential decay.

## 6. Conclusions

In this paper, we applied the Contact Dynamics Method, as a variant of DEM, together with a Bonded Cell Method for particle breakage with polygonal particles in 2D to investigate the grinding process of granular materials in a simulated ball mill geometry. The particle size reduction and evolution of the specific surface were investigated in two series of simulations. In the first serie, the ball size was varied with a constant total volume of balls. In the second one, the number of balls was varied with a constant ball size. In both cases, the number and sizes of powder particles was kept constant.

We showed that, when the total volume of grinding balls is kept constant, changing the ball size has little effect on the evolution of grinding since the total kinetic energy is proportional to the total volume and hence it has nearly the same value in all simulations. For the extreme values of ball size (close to the size of powder grains or too large compared to the total volume of powder) correspond to special flow regimes that govern the grinding behavior and hence the behavior is special. We also found that the grinding rate increases with the number of balls of the same size, but this trend is counterbalanced by energy dissipation due to inelastic collisions between balls for a large number of balls. There is therefore an optimal number of grinding balls for which the grinding rate has its largest value.

We also introduced a population balance model by dividing the particles into three populations (big, medium and small) and evaluated its parameters from the simulations. We found that the first breakage events that take place in our systems are big particles turning into medium ones. Furthermore, the breakage rate of big particles into medium ones was found to be nearly the same as the breakage rate from medium into small sizes. At first order, the particle volumes follow almost an exponential decay during grinding but the volume change rates of big and medium particles are not exactly constant as a result of the cushioning effect. By including the cushioning effect, a good agreement was found with the simulation results in both case studies.

In this work, we kept constant values of material parameters in order to focus more specifically on the effects of the grinding media and the grinding process itself. Further investigation is necessary to evaluate the scaling of the grinding process with parameters such as fracture energy and stress as well as the filling rate. For example, the low number of small fragments generated from big particles reflects low erosion and shattering effects. It is thus interesting to see how robust is this behavior with respect to the material parameters of the process. In the same way, the effect of the ratio  $C_t/C_n$  needs to be investigated. Previous simulations seem to indicate that the dynamic fracture of individual particles by impact is only marginally affected by this parameter [29]. The ternary model of population balance is obviously a rough description of the evolution of particle volumes. But it can be extended to larger numbers of populations although it will involve larger numbers of rates and parameters to be determined.

The focus of this paper was on the parametric analysis of the effects of grinding media on the reduction process with some insights from the local mechanisms such as force chains appearing between balls when their volume fraction is high. This analysis can be pursued by investigating in more detail the local mechanisms of breakage and its correlations with force chains for powder particles [46]. Such an investigation requires, however, a spatio-temporal approach as the flow is strongly inhomogeneous and the force chains have different lifetimes. They also evolve in time with grinding. In a similar vein, the dominant modes of particle breakage can be investigated in different parts of the flow.

Finally, the insights provided by our simulations call also for new experiments in view of validating the simulation method employed in this work. In particular, a systematic investigation of the influence of the number of balls on the grinding process seems to be accessible to experiments. Such experiments do not need to be long since the initial grinding rate provides a discriminating variable that can be measured from either specific surface or mean particle size. The 2D nature of our simulations does not allow for a strict comparison with experiments, but it is important to keep the same values of drum diameter and Froude number, which are important for the flow regime.

## References

- [1] L. G. Austin, P. Bagga, M. Celik, Breakage properties of some materials in a laboratory ball mill, *Powder Technology* 28 (2) (1981) 235–243. doi: 10.1016/0032-5910(81)87049-0.
- [2] S. Agrawala, R. Rajamani, P. Songfack, B. Mishra, Mechanics of media motion in tumbling mills with 3d discrete element method, *Minerals Engineering* 10 (2) (1997) 215–227. doi: 10.1016/S0892-6875(96)00147-1.
- [3] D. W. Fuerstenau, A. Z. Abouzeid, The energy efficiency of ball milling in comminution, *International Journal of Mineral Processing* 67 (1-4) (2002) 161–185. doi: 10.1016/S0301-7516(02)00039-X.

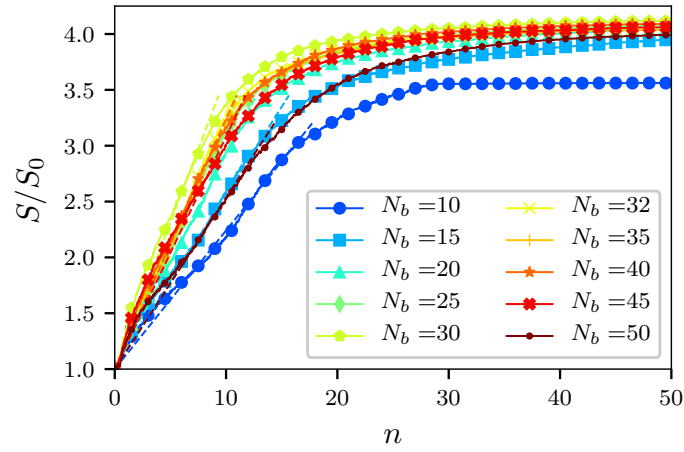
- [4] D. Tromans, Mineral comminution: Energy efficiency considerations, *Minerals Engineering* 21 (8) (2008) 613–620. doi:10.1016/j.mineng.2007.12.003.
- [5] G. R. Ballantyne, M. S. Powell, M. Tiang, Proportion of energy attributable to comminution, *Proceedings of the 11th Australasian Institute of Mining and Metallurgy Mill Operator’s Conference* (October) (2012) 25–30.
- [6] A. S. Erdem, S. L. Ergün, The effect of ball size on breakage rate parameter in a pilot scale ball mill, *Minerals Engineering* 22 (7-8) (2009) 660–664. doi:10.1016/j.mineng.2009.01.015.  
URL <http://dx.doi.org/10.1016/j.mineng.2009.01.015>
- [7] M. J. Metzger, S. P. Desai, D. Glasser, D. Hildebrandt, B. J. Glasser, Using the attainable region analysis to determine the effect of process parameters on breakage in a ball mill, *AIChE Journal* 58 (9) (2012) 2665–2673. doi:10.1002/aic.12792.  
URL <http://doi.wiley.com/10.1002/aic.12792>
- [8] D. M. Francioli, Effect of operational variables on ball milling, Ph.D. thesis, UFRJ/ Escola Politécnica (2015).
- [9] V. K. Gupta, Effect of size distribution of the particulate material on the specific breakage rate of particles in dry ball milling, *Powder Technology* 305 (2017) 714–722. doi:10.1016/j.powtec.2016.10.075.  
URL <http://dx.doi.org/10.1016/j.powtec.2016.10.075>
- [10] L. Vogel, W. Peukert, From single particle impact behaviour to modelling of impact mills, *Chemical Engineering Science* 60 (18) (2005) 5164–5176. doi:10.1016/j.ces.2005.03.064.
- [11] L. M. Tavares, R. M. de Carvalho, Modeling breakage rates of coarse particles in ball mills, *Minerals Engineering* 22 (7-8) (2009) 650–659. doi:10.1016/j.mineng.2009.03.015.  
URL <http://dx.doi.org/10.1016/j.mineng.2009.03.015>
- [12] V. K. Gupta, S. Sharma, Analysis of ball mill grinding operation using mill power specific kinetic parameters, *Advanced Powder Technology* 25 (2) (2014) 625–634. doi:10.1016/j.apt.2013.10.003.  
URL <http://dx.doi.org/10.1016/j.apt.2013.10.003>
- [13] B. Caicedo, M. Ocampo, L. Vallejo, Modelling comminution of granular materials using a linear packing model and Markovian processes, *Computers and Geotechnics* 80 (2016) 383–396. doi:10.1016/j.compgeo.2016.01.022.  
URL <http://dx.doi.org/10.1016/j.compgeo.2016.01.022>

- [14] L. Tavares, R. King, Single-particle fracture under impact loading, *International Journal of Mineral Processing* 54 (July) (1998) 1–28. doi:10.1016/S0301-7516(98)00005-2.
- [15] C. Chi, Y. Qi, Y. Long, D. G. Papadopoulos, A. C. Bentham, M. Ghadiri, Development of a novel approach towards predicting the milling behaviour of pharmaceutical powders 23 (2004) 327–336. doi:10.1016/j.ejps.2004.08.006.
- [16] E. Bilgili, J. Yepes, B. Scarlett, Formulation of a non-linear framework for population balance modeling of batch grinding: Beyond first-order kinetics, *Chemical Engineering Science* 61 (1) (2006) 33–44. doi:10.1016/j.ces.2004.11.060.
- [17] M. Capece, R. N. Davé, E. Bilgili, On the origin of non-linear breakage kinetics in dry milling, *Powder Technology* 272 (2015) 189–203. doi:10.1016/j.powtec.2014.11.040.  
URL <http://dx.doi.org/10.1016/j.powtec.2014.11.040>
- [18] H. Lee, H. Cho, J. Kwon, Using the discrete element method to analyze the breakage rate in a centrifugal/vibration mill, *Powder Technology* 198 (3) (2010) 364–372. doi:10.1016/j.powtec.2009.12.001.  
URL <http://dx.doi.org/10.1016/j.powtec.2009.12.001>
- [19] M. S. Powell, N. S. Weerasekara, S. Cole, R. D. Laroche, J. Favier, DEM modelling of liner evolution and its influence on grinding rate in ball mills, *Minerals Engineering* 24 (3-4) (2011) 341–351. doi:10.1016/j.mineng.2010.12.012.  
URL <http://dx.doi.org/10.1016/j.mineng.2010.12.012>
- [20] M. H. Wang, R. Y. Yang, A. B. Yu, DEM investigation of energy distribution and particle breakage in tumbling ball mills, *Powder Technology* 223 (2012) 83–91. doi:10.1016/j.powtec.2011.07.024.
- [21] N. S. Weerasekara, L. X. Liu, M. S. Powell, Estimating energy in grinding using DEM modelling, *Minerals Engineering* 85 (2016) 23–33. doi:10.1016/j.mineng.2015.10.013.  
URL <http://dx.doi.org/10.1016/j.mineng.2015.10.013>
- [22] N. Jiménez-Herrera, G. K. Barrios, L. M. Tavares, Comparison of breakage models in DEM in simulating impact on particle beds, *Advanced Powder Technology* 29 (3) (2018) 692–706. doi:10.1016/j.apt.2017.12.006.
- [23] M. J. Metzger, B. J. Glasser, Simulation of the breakage of bonded agglomerates in a ball mill, *Powder Technology* 237 (2013) 286–302. doi:10.1016/j.powtec.2012.12.006.  
URL <http://dx.doi.org/10.1016/j.powtec.2012.12.006>

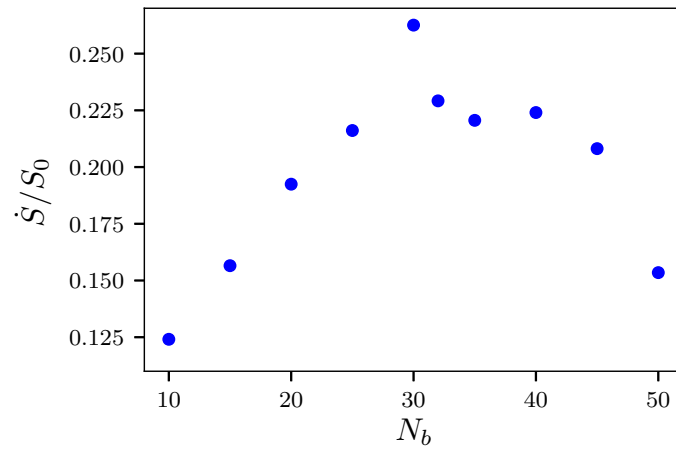
- [24] P. W. Cleary, Recent advances in DEM modelling of tumbling mills, *Minerals Engineering* 14 (10) (2001) 1295–1319. doi:10.1016/S0892-6875(01)00145-5.
- [25] P. W. Cleary, R. D. Morrison, G. W. Delaney, Incremental damage and particle size reduction in a pilot SAG mill: DEM breakage method extension and validation, *Minerals Engineering* 128 (August) (2018) 56–68. doi:10.1016/j.mineng.2018.08.021. URL <https://doi.org/10.1016/j.mineng.2018.08.021>
- [26] G. W. Delaney, P. W. Cleary, M. D. Sinnott, R. D. Morrison, Novel application of DEM to modelling comminution processes, *IOP Conference Series: Materials Science and Engineering* 10 (1) (2010). doi:10.1088/1757-899X/10/1/012099.
- [27] D. H. Nguyen, E. Azéma, P. Sornay, F. Radjai, Bonded-cell model for particle fracture, *Physical Review E - Statistical, Nonlinear, and Soft Matter Physics* 91 (2) (2015). doi:10.1103/PhysRevE.91.022203.
- [28] D. Cantor, E. Azéma, P. Sornay, F. Radjai, Three-dimensional bonded-cell model for grain fragmentation, *Computational Particle Mechanics* (2016). doi:10.1007/s40571-016-0129-0. URL <http://link.springer.com/10.1007/s40571-016-0129-0>
- [29] L. F. Orozco, J. Y. Delenne, P. Sornay, F. Radjai, Discrete-element model for dynamic fracture of a single particle, *International Journal of Solids and Structures* 166 (2019) 47–56. doi:10.1016/j.ijsolstr.2019.01.033.
- [30] D.-H. Nguyen, E. Azéma, F. Radjai, Evolution of particle size distributions in crushable granular materials, *Geomechanics from Micro to Macro* (2015) 275–280 doi:doi:10.1201/b17395-48\r10.1201/b17395-48.
- [31] J. J. Moreau, Some numerical methods in multibody dynamics: application to granular materials, *European journal of mechanics. A. Solids* 13 (A/Solids) (1994) 93–114.
- [32] V. Acary, B. Brogliato, Numerical Methods for Nonsmooth Dynamical Systems, Vol. 35 of *Lecture Notes in Applied and Computational Mechanics*, Springer Berlin Heidelberg, Berlin, Heidelberg, 2008. doi:10.1007/978-3-540-75392-6.
- [33] F. Radjai, V. Richefeu, Contact dynamics as a nonsmooth discrete element method, *Mechanics of Materials* 41 (6) (2009) 715–728. doi:10.1016/j.mechmat.2009.01.028. URL <http://dx.doi.org/10.1016/j.mechmat.2009.01.028>
- [34] F. Radjai, F. Dubois (Eds.), *Discrete-Element Modeling of Granular Materials*, Wiley-ISTE, New-York, 2011, iSBN: 978-1-84821-260-2.

- [35] J. Nakayama, Direct Measurement of Fracture Energies of Brittle Heterogeneous Materials, *Journal of the American Ceramic Society* 48 (11) (1965) 583–587. doi:10.1111/j.1151-2916.1965.tb14677.x.
- [36] P. S. Maiya, Surface diffusion, surface free energy, and grain-boundary free energy of Uranium Dioxide, *J. Nucl. Mater.* 40 (1071) (1971) 57. doi:10.1016/0022-3115(71)90116-4.
- [37] D. H. Nguyen, E. Azéma, F. Radjai, P. Sornay, Effect of size polydispersity versus particle shape in dense granular media, *Physical Review E - Statistical, Nonlinear, and Soft Matter Physics* 90 (1) (2014) 1–12. doi:10.1103/PhysRevE.90.012202.
- [38] N. Gui, X. Yang, J. Tu, S. Jiang, Numerical simulation and analysis of mixing of polygonal particles in 2D rotating drums by SIPHPM method, *Powder Technology* 318 (2017) 248–262. doi:10.1016/j.powtec.2017.06.007.  
URL <http://dx.doi.org/10.1016/j.powtec.2017.06.007>
- [39] Y. Wu, X. An, Q. Qian, L. Wang, A. Yu, Dynamic modelling on the confined crystallization of mono-sized cubic particles under mechanical vibration, *The European Physical Journal E* 41 (11) (2018) 139. doi:10.1140/epje/i2018-11744-2.  
URL <http://link.springer.com/10.1140/epje/i2018-11744-2>
- [40] J. Mellmann, The transverse motion of solids in rotating cylinders-forms of motion and transition behavior, *Powder Technology* 118 (3) (2001) 251–270. doi:10.1016/S0032-5910(00)00402-2.
- [41] I. Govender, Granular flows in rotating drums: A rheological perspective, *Minerals Engineering* 92 (2016) 168–175. doi:10.1016/j.mineng.2016.03.021.
- [42] R. M. De Carvalho, L. M. Tavares, Predicting the effect of operating and design variables on breakage rates using the mechanistic ball mill model, *Minerals Engineering* 43-44 (2013) 91–101. doi:10.1016/j.mineng.2012.09.008.  
URL <http://dx.doi.org/10.1016/j.mineng.2012.09.008>
- [43] C. Sammis, G. King, R. Biegel, The kinematics of gouge deformation, *Pure and applied geophysics* 125 (5) (1987) 777–812. doi:10.1007/BF00878033.
- [44] C. Voivret, Cushioning effect in highly polydisperse granular media, *AIP Conference Proceedings* 1542 (June) (2013) 405–408. doi:10.1063/1.4811953.
- [45] O. Tsoungui, D. Vallet, J. C. Charmet, Numerical model of crushing of grains inside two-dimensional granular materials, *Powder Technology* 105 (1-3) (1999) 190–198. doi:10.1016/S0032-5910(99)00137-0.

- [46] W. Wu, G. Ma, W. Zhou, D. Wang, X. Chang, Force transmission and anisotropic characteristics of sheared granular materials with rolling resistance, *Granular Matter* 21 (4) (2019) 88. doi:10.1007/s10035-019-0938-y.  
URL <https://doi.org/10.1007/s10035-019-0938-y>



(a)



(b)

Figure 10: a) Evolution of the normalized specific surface as a function of the number of drum rotations for different numbers of balls  $N_b$ , and b) Grinding rate  $\dot{S}$  normalized by the initial value  $S_0$  of specific surface during the first 20 drum rotations as a function of the number of balls.

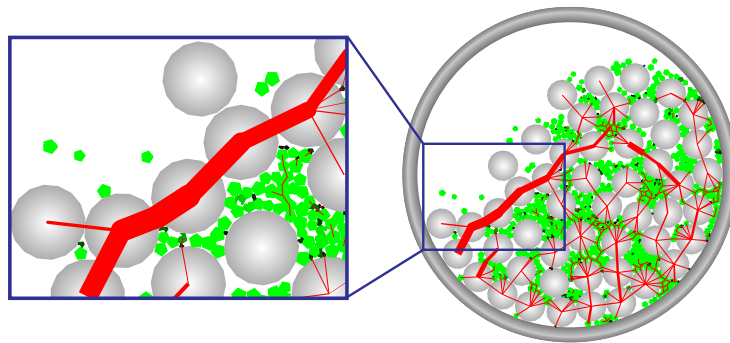
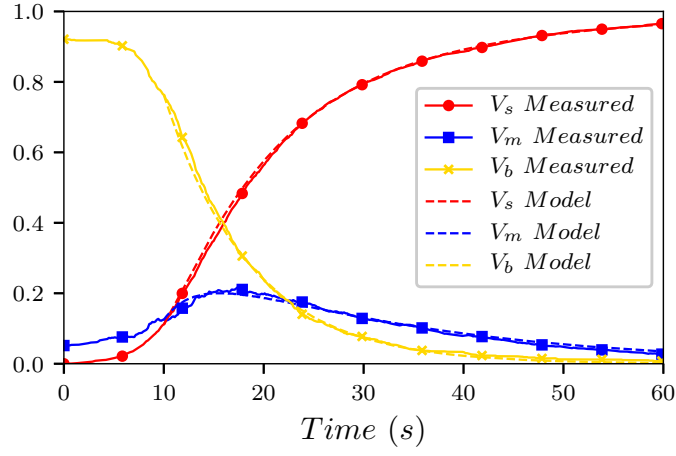
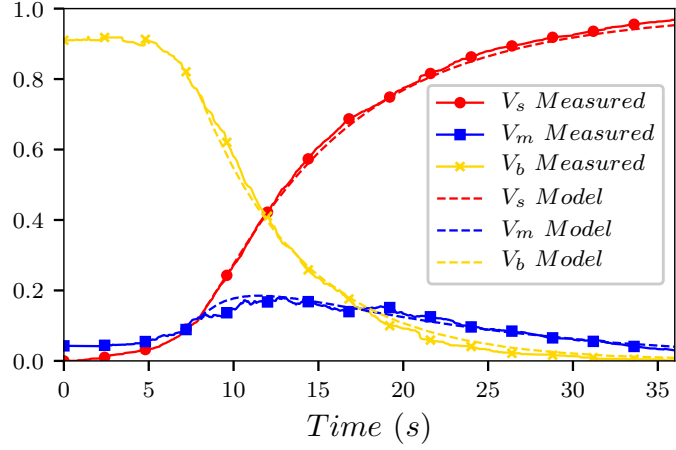


Figure 11: A snapshot of force chains in a simulation with  $N_b = 50$  grinding balls. Red line thickness is proportional to normal force. We observe both binary collisions and chains of impulsive (short-lived) forces.

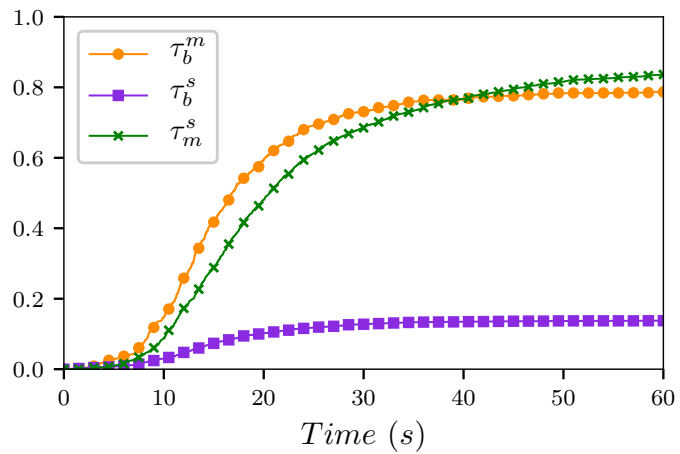


(a)

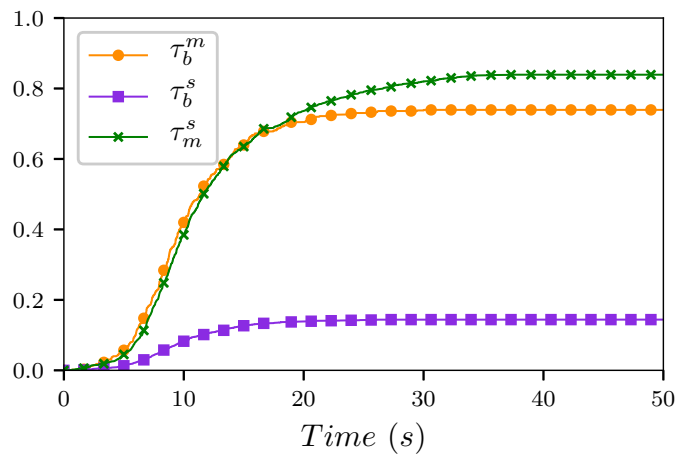


(b)

Figure 12: Time evolution of the volume of each size population normalized by the total volume  $V$  for a)  $D_b = 15$  and b)  $N_b = 32$ . The dashed lines are analytical fits obtained from the system of equations 8.



(a)



(b)

Figure 13: Cumulative volume transfers: from big to small ( $\tau_b^s$ ), from big to medium ( $\tau_b^m$ ), and from medium to small ( $\tau_m^s$ ), for a)  $D_b = 15$  and b)  $N_b = 32$ .